Int. J. Electron. Commun. (AEÜ) 153 (2022) 154293

Contents lists available at ScienceDirect

Int. J. Electron. Commun. (AEÜ)

journal homepage: www.elsevier.com/locate/aeue

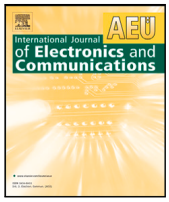

Regular paper

A compact model of the ZARC for circuit simulators in the frequency and time domains

Juan A. López-Villanueva [a,b,*], Pablo Rodríguez-Iturriaga [a], Luis Parrilla [a], Salvador Rodríguez-Bolívar [a,b]

[a] Department of Electronics and Computer Technology, Faculty of Sciences, University of Granada, Campus Fuentenueva, Granada, 18071, Spain
[b] CITIC, University of Granada, Periodista Rafael Gomez Montero, 2, Granada, 18014, Spain

ARTICLE INFO

MSC:
26A33
44A10

Keywords:
Fractional-order circuits
ZARC
Equivalent-circuit model
SPICE

ABSTRACT

Equivalent-circuit models containing fractional-order elements are often employed to make use of fractional-order calculus in the frequency and time domains in a variety of applications. Many of these circuits contain constant-phase elements that appear in parallel with a resistor in a configuration called ZARC. But to avoid fractional order derivatives and include it in circuit simulators, the ZARC itself can also be replaced by equivalent circuit models that only contain integer order elements, such as resistors and capacitors. In this article, a novel compact model is presented to substitute the ZARC by a multiple-RC network. This model is valid for a continuous value of the order exponent and is applicable over a very wide range of frequencies, making it useful in both the frequency and time domains. Since it uses only basic functions and operators, it has been easily implemented as a subcircuit in circuit simulators. The validity of the model has been verified and it has been compared with some previously proposed passive circuit models. The model has also been discussed in relation to the initialization problem, which is an often overlooked challenge in fractional-order circuits.

1. Introduction

Fractional-order calculus is gaining great interest as it is finding its application in a variety of disciplines in the last decades [1–5]. In many of them, fractional-order differential equations are represented by equivalent-circuit models that contain fractional-order elements [6] with an electrical impedance that depends on frequency according to a non-integer power law. A key component is the constant-phase element (CPE) [7–9], also called fractional-order capacitor [10], which is unequivocally observed in experimental results obtained with electrochemical impedance measurements [11]. The CPE name recognizes the fact that its phase response is constant over the entire frequency range. It has been identified separately as in the case of the so called Warburg impedance in battery models [8,12] or as part of a larger model that also contains other elements. A very common configuration used in fractional-order circuit models is the ZARC, composed of a CPE connected in parallel with a resistor [13], as shown in Fig. 1(a). It is widely used in models of batteries and supercapacitors [8,14–17] and also in other applications such as in models used to explain bioelectric phenomena [4,18].

Many scientists and engineers use fractional order models in the frequency and Laplace domains to represent the electrochemical impedance spectroscopy (EIS) results [11] or to design fractional-order controllers [19,20]. There is also great interest in applying them in the time domain [21–23]. However, time derivatives of non-integer order make these models particularly challenging. Time-domain analysis is also necessary to include fractional-order element models in circuit simulation tools such as SPICE or PSIM [24]. This has motivated a great research effort to obtain accurate approximations to replace CPE or ZARC elements by equivalent circuits that only include integer-order elements. The aim of the present work is to provide a useful model in this context, which, despite our initial interest in the field of electrochemical modeling, can be expressed in a general way so that it can be applied in a wider range of applications.

Several methods exist in the literature to obtain integer-order passive approximations to the CPE or the ZARC. Oustaloup et al. [25] proposed a method to synthesize the transfer function of the fractional element by a recursive distribution of zeros and poles within a predetermined frequency range. This approach has been widely adopted by other authors [22,26]. Tsirimokou [10] reviewed some methods

* Corresponding author at: Department of Electronics and Computer Technology, Faculty of Sciences, University of Granada, Campus Fuentenueva, Granada, 18071, Spain.
E-mail address: jalopez@ugr.es (J.A. López-Villanueva).

https://doi.org/10.1016/j.aeue.2022.154293
Received 11 April 2022; Accepted 18 June 2022
Available online 22 June 2022

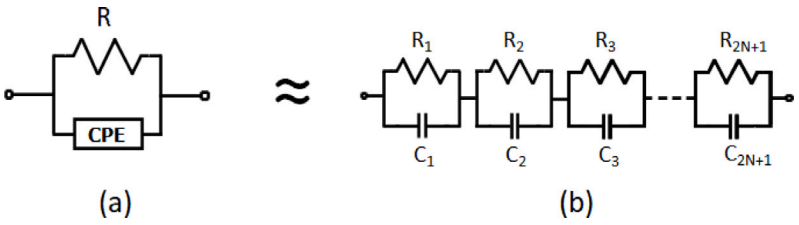

Fig. 1. (a) The ZARC. (b) Approximation by a multiple RC network.

for obtaining rational approximations of the fractional order transfer function and used the continued fraction expansion method to obtain the component values of different circuit topologies such as Foster I, Foster II, Cauer I and Cauer II. Other authors have also considered these topologies [6,27]. A related approach, common in the battery modeling literature [28], consists of approximating the impedance of the fractional-order element with a series of parallel RC branches, but instead of synthesizing a rational transfer function, the impedance of the fractional element as a function of frequency is directly approximated by that of the RC circuit. This network is shown in Fig. 1(b), with an odd number of RC elements. It is similar to the Foster I topology, although the Foster I circuit adds a series resistor that limits its accuracy to a region of frequencies between two extreme values. However, it has allowed to Tsirimokou [10] to obtain a very accurate model within a wide frequency range.

Farmann et al. [15] approximated the ZARC by three and five RC elements in series, obtaining a better accuracy with the five-element network. Kim et al. [24] also considered three RC elements. Heil and Jossen [29] introduced two approaches to approximate the ZARC by RC circuits. An infinite number of series-connected RC circuits that can be related to ZARC by explicit equations is considered in the first method, and the second one uses just three series-connected RC circuits, but adds a minimization procedure to obtain the component values. Agudelo et al. [30] compared the high-order integer transfer function by Oustaloup et al. and the multiple RC circuit in terms of accuracy and computational burden and concluded that the multiple-RC approach offers the best compromise between accuracy and complexity. As the series combination of parallel RC elements is commonly used in battery modeling, and methods with this model are well established in the battery literature [12], we have chosen the series of parallel RC branches as a model to approximate the ZARC in this work.

Authors that approximate the fractional-order element by an integer-order circuit often provide a table with the component parameters for a discrete set of values of the fractional exponent [15,24,29,30]. However, a compact model valid for any arbitrary order is highly desirable, as it could be applied in computational procedures where the order value could vary continuously, such as in optimization methods used to fit the fractional-order parameters to experimental results, or in defining subcircuit models for circuit simulators in which the fractional-order exponent acts as an input parameter. The simplicity of the model would be an added value for the latter application. Oustaloup et al. [25] developed a procedure to approximate the CPE with a continuous variation of the order exponent. Tsirimokou [10] proposed and implemented in Matlab a model applicable to any value of the order exponent in the range $0 < \alpha < 1$, which uses the residue function included in Matlab/Octave to implement the fraction expansion method. In this paper, we propose an alternative model for the same range of the order exponent, which is valid for all frequencies and only uses basic functions and operators, so that it can easily be implemented in circuit simulators and requires less computation time. Taking the fractional order, the resistance and the time constant as the three input parameters of the ZARC model, the values of the RC-circuit components are directly calculated. To develop the model, we have compared the behavior of the ZARC and the multiple-RC circuit in detail, both in the frequency and the time domains, and have obtained simple models to be used as Octave/Matlab functions or SPICE subcircuits.

The outline of this paper is as follows. The behavior of the ZARC in the frequency and time domains is detailed in Section 2, and it is compared with that of the multiple RC approximation in Section 3. The compact model based on 5RC and 7RC approximations is described in Section 4, and some results are shown. Section 5 explains how our proposed model deals with the initialization of the ZARC, and some concluding remarks are finally provided in Section 6.

2. The ZARC in the frequency and time domains

The ZARC is composed of a constant-phase element (CPE) connected in parallel with a resistor R. Since the impedance of the CPE in the Laplace domain is [8,9]

$$Z_{CPE}(s) = \frac{1}{Qs^{\alpha}}, \tag{1}$$

where α is the fractional-order exponent and Q is the capacity coefficient or pseudo-capacitance. Then, the impedance for the ZARC is obtained as

$$Z_{\alpha}(s) = \frac{Z_{CPE}\,R}{Z_{CPE}+R} = \frac{R}{1+RQs^{\alpha}}. \tag{2}$$

To avoid fractional dimensions in parameter Q, it is useful to define a time constant as

$$\tau \equiv (RQ)^{\frac{1}{\alpha}}, \tag{3}$$

so that

$$Z_{\alpha}(s) = \frac{R}{1+(\tau s)^{\alpha}}. \tag{4}$$

This expression for the impedance in the Laplace domain will be used as a starting point in the next two subsections.

2.1. Frequency domain

To analyze the frequency response of the ZARC, we substitute $s = j\omega$, with $j = \sqrt{-1}$, in (4), thus obtaining

$$Z_{\alpha}(j\omega) = \frac{R}{1+(j\omega\tau)^{\alpha}}. \tag{5}$$

Since $j^{\alpha} = e^{j\alpha\frac{\pi}{2}} = cos\left(\alpha\frac{\pi}{2}\right) + jsin\left(\alpha\frac{\pi}{2}\right)$, we can write (5) as

$$Z_{\alpha} = R_{\alpha} - jX_{\alpha}, \tag{6}$$

where

$$R_{\alpha}(\omega) = \frac{R\left[1+(\omega\tau)^{\alpha}cos\left(\alpha\frac{\pi}{2}\right)\right]}{1+(\omega\tau)^{2\alpha}+2(\omega\tau)^{\alpha}cos\left(\alpha\frac{\pi}{2}\right)} \tag{7}$$

and

$$X_{\alpha}(\omega) = \frac{R(\omega\tau)^{\alpha}sin\left(\alpha\frac{\pi}{2}\right)}{1+(\omega\tau)^{2\alpha}+2(\omega\tau)^{\alpha}cos\left(\alpha\frac{\pi}{2}\right)}. \tag{8}$$

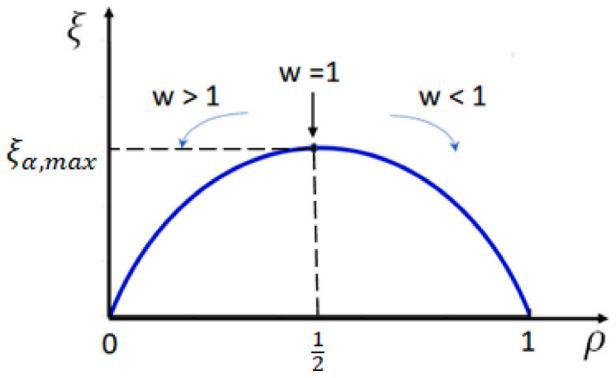

Fig. 2. Nyquist plot for the normalized reactance and resistance of the ZARC.

To obtain a manageable model, it is convenient to express (7) and (8) in normalized dimensionless form so that they only depend on the exponent of order α and on dimensionless magnitudes. For this purpose, we define

$$w \equiv \omega\tau \ , \ \rho_\alpha(w) \equiv \frac{R_\alpha}{R} \ , \ \xi_\alpha(w) \equiv \frac{X_\alpha}{R}, \tag{9}$$

thus obtaining

$$\rho_\alpha(w) = \frac{1 + w^\alpha cos\left(\alpha\frac{\pi}{2}\right)}{1 + w^{2\alpha} + 2w^\alpha cos\left(\alpha\frac{\pi}{2}\right)} \tag{10}$$

and

$$\xi_\alpha(w) = \frac{w^\alpha sin\left(\alpha\frac{\pi}{2}\right)}{1 + w^{2\alpha} + 2w^\alpha cos\left(\alpha\frac{\pi}{2}\right)}. \tag{11}$$

The maximum value of the normalized reactance ξ_α is obtained when $w = 1$, and its value is

$$\xi_{\alpha,max} = \xi_\alpha(w = 1) = \frac{sin\left(\alpha\frac{\pi}{2}\right)}{2\left[1 + cos\left(\alpha\frac{\pi}{2}\right)\right]}. \tag{12}$$

The normalized resistance at this frequency is $\rho_\alpha(w = 1) = \frac{1}{2}$.

The Nyquist plot for the normalized reactance and resistance is shown in Fig. 2.

Eqs. (10) and (11) have the limits

$$w \to 0 \ \Rightarrow \ \rho_\alpha \to 1 \ , \ \xi_\alpha \to 0,$$
$$w \to \infty \ \Rightarrow \ \rho_\alpha \to 0 \ , \ \xi_\alpha \to 0,$$

and the symmetry properties

$$\rho_\alpha(w) + \rho_\alpha(\frac{1}{w}) = 1, \tag{13}$$

$$\xi_\alpha(w) = \xi_\alpha(\frac{1}{w}). \tag{14}$$

These properties have also been pointed out by previous authors [29], and will be compared to that of the multiple RC approximation in next section.

2.2. Time domain

Eq. (4) is also used in this subsection to analyze the time behavior of the ZARC. The voltage–current relationship in the Laplace domain is

$$V(s) = I(s)Z_\alpha(s), \tag{15}$$

so that the voltage–current relationship in the time domain can be written as a convolution product [31],

$$v(t) = i(t) * z_\alpha(t), \tag{16}$$

where $*$ stands for the convolution product of the two magnitudes, and $z_\alpha(t)$ is the inverse Laplace transform of impedance $Z_\alpha(s)$

$$z_\alpha(t) = \mathcal{L}^{-1}\left[Z_\alpha(s)\right]. \tag{17}$$

The inverse Laplace transform of the ZARC impedance can be obtained as [1,19]

$$z_\alpha(t) = \mathcal{L}^{-1}\left[\frac{R}{1 + (\tau s)^\alpha}\right] = \frac{R}{\tau^\alpha}t^{\alpha-1}E_{\alpha,\alpha}\left[-\left(\frac{t}{\tau}\right)^\alpha\right], \tag{18}$$

where $E_{\alpha,\alpha}$ is the two-parameter Mittag-Leffler function [1,19], defined according to

$$E_{\alpha,\beta}(x) = \sum_{n=0}^{\infty}\frac{x^n}{\Gamma[n\alpha + \beta]}, \tag{19}$$

and $\Gamma(x)$ is the Gamma function.

The convolution expression (16) is then written as

$$v(t) = \int_0^t i(u)\frac{R}{\tau}\left(\frac{t-u}{\tau}\right)^{\alpha-1}E_{\alpha,\alpha}\left[-\left(\frac{t-u}{\tau}\right)^\alpha\right]du. \tag{20}$$

where u is a dummy variable. This equation has been obtained by other authors [1,30], but it can be more conveniently written as follows.

If the one-parameter Mittag-Leffler function is defined as [1]

$$E_\alpha(x) = \sum_{n=0}^{\infty}\frac{x^n}{\Gamma(n\alpha + 1)}, \tag{21}$$

we can easily obtain the following property

$$E_{\alpha,\alpha}(x) = \alpha\frac{dE_\alpha(x)}{dx}. \tag{22}$$

Then, Eq. (20) is finally written as

$$v(t) = R\int_0^t i(u)\frac{d}{du}E_\alpha\left[-\left(\frac{t-u}{\tau}\right)^\alpha\right]du. \tag{23}$$

This is a useful result in practice, since if the electrical current, $i(t)$, can be approximated by a piecewise constant function, the voltage is readily obtained. We will apply it in Section 5 below.

3. Behavior of the multiple RC network

We will analyze a network with an odd number of RC elements, such as shown in Fig. 1(b). The total impedance in the Laplace domain is

$$Z_{RC}(s) = \sum_{k=1}^{2N+1}\frac{R_k}{1 + \tau_k s}, \tag{24}$$

with

$$\tau_k \equiv R_k C_k. \tag{25}$$

We will proceed in the same way as we have done with the ZARC in the previous Section.

3.1. Frequency domain

We again substitute $s = j\omega$ in (24) obtaining

$$Z_{RC}(j\omega) = \sum_{k=1}^{2N+1}\frac{R_k}{1 + j\omega\tau_k}. \tag{26}$$

If Eq. (26) is separated into its real and imaginary parts,

$$Z_{RC}(j\omega) = R_{RC}(\omega) - jX_{RC}(\omega), \tag{27}$$

then

$$R_{RC}(\omega) = \sum_{k=1}^{2N+1}\frac{R_k}{1 + (\omega\tau_k)^2} \tag{28}$$

and

$$X_{RC}(\omega) = \sum_{k=1}^{2N+1} \frac{R_k \omega \tau_k}{1 + (\omega \tau_k)^2}. \tag{29}$$

We also normalize with $w \equiv \omega\tau$, where τ is still the time constant of the ZARC in order to be able to compare both models easily, and define the normalized resistance and reactance by also dividing by the resistance of the ZARC, R, according to

$$\rho_{RC}(w) \equiv \frac{R_{RC}(w)}{R}\ ,\ \xi_{RC}(w) \equiv \frac{X_{RC}(w)}{R} \tag{30}$$

and also define the normalized resistances and time constant according to (31)

$$r_k \equiv \frac{R_k}{R}\ ,\ t_k \equiv \frac{\tau_k}{\tau}. \tag{31}$$

The result is

$$\rho_{RC}(w) = \sum_{k=1}^{2N+1} \frac{r_k}{1 + (w t_k)^2} \tag{32}$$

$$\xi_{RC}(w) = \sum_{k=1}^{2N+1} \frac{r_k w t_k}{1 + (w t_k)^2} \tag{33}$$

To approximate Eqs. (10) and (11) by Eqs. (32) and (33), respectively, we impose that the two models, ZARC and multiple RC, have the same limits

$$\lim_{w\to 0} \xi_{RC} = \lim_{w\to \infty} \xi_{RC} = 0 \tag{34}$$

$$\lim_{w\to \infty} \rho_{RC} = 0,\ \lim_{w\to 0} \rho_{RC} = 1 \tag{35}$$

and the same symmetry properties (13) and (14). This is achieved by imposing [30]

$$\sum_{k=1}^{2N+1} r_k = 1, \tag{36}$$

and

$$r_k = r_{2N+2-k}\ ,\ t_k = \frac{1}{t_{2N+2-k}}, \tag{37}$$

so that the parameters of the central element are

$$r_{N+1} = 1 - \sum_{k=1}^{N} 2r_k\ ,\ t_{N+1} = 1. \tag{38}$$

Then, instead of $2N + 1$ terms and $4N + 2$ free parameters, we are left with N+1 terms and 2N parameters for a network with 2N+1 RC elements. The final result is

$$\rho_{RC}(w) = \frac{1}{1+w^2} + \sum_{k=1}^{N} r_k \left[\frac{1}{1 + w^2 t_k^2} + \frac{{t_k}^2}{{t_k}^2 + w^2} - \frac{2}{1+w^2}\right], \tag{39}$$

$$\xi_{RC}(w) = \frac{w}{1+w^2} + \sum_{k=1}^{N} r_k w \left[\frac{t_k}{1 + w^2 t_k^2} + \frac{t_k}{{t_k}^2 + w^2} - \frac{2}{1+w^2}\right] \tag{40}$$

The values of the parameters r_k and t_k should be chosen so that Eqs. (39) and (40) are as close as possible to Eqs. (10) and (11), respectively, in all the range of w for every value of the order exponent α.

3.2. Time domain

As we have done in Section 2.2, we consider the voltage–current relationship in the Laplace domain,

$$V(s) = I(s) Z_{RC}(s), \tag{41}$$

and write the voltage as a function of time in terms of a convolution integral

$$v(t) = i(t) * z_{RC}(t) = \int_0^t i(u) z_{RC}(t-u) du, \tag{42}$$

where

$$z_{RC}(t) = \mathcal{L}^{-1}\left[Z_{RC}(s)\right] = \sum_{k=1}^{2N+1} R_k \mathcal{L}^{-1}\left[\frac{1}{1+\tau_k s}\right], \tag{43}$$

whose result is

$$z_{RC}(t) = \sum_{k=1}^{2N+1} \frac{R_k}{\tau_k} exp\left(-\frac{t}{\tau_k}\right). \tag{44}$$

We observe that

$$z_{RC}(t-u) = \sum_{k=1}^{2N+1} \frac{R_k}{\tau_k} exp\left(-\frac{t-u}{\tau_k}\right) = \frac{d}{du} \sum_{k=1}^{2N+1} R_k exp\left(-\frac{t-u}{\tau_k}\right) \tag{45}$$

so that, if we define the function F_{2N+1} as

$$F_{2N+1}(x) = \sum_{k=1}^{2N+1} r_k exp\left(-\frac{x}{t_k}\right), \tag{46}$$

then

$$F_{2N+1}\left(\frac{t-u}{\tau}\right) \equiv \sum_{k=1}^{2N+1} r_k exp\left(-\frac{t-u}{\tau_k}\right) \tag{47}$$

where we have used $\tau_k = \tau t_k$ according to Eq. (31).

We can thus express Eq. (42) for the voltage as a function of time in a way similar to Eq. (23):

$$v(t) = R \int_0^t i(u) \frac{d}{du} F_{2N+1}\left(\frac{t-u}{\tau}\right) du \tag{48}$$

Eqs. (23) and (48) give us the same time dependence of the voltage provided that we can approximate

$$E_\alpha(-x^\alpha) \approx F_{2N+1}(x), \tag{49}$$

where Eq. (46), with the symmetry relations (37) and (38), reduces to

$$F_{2N+1}(x) = e^{-x} - \sum_{k=1}^{N} r_k \left(2e^{-x} - e^{-\frac{x}{t_k}} - e^{-x t_k}\right). \tag{50}$$

We will test the validity of the approximation (49) in next section. This is an interesting point, since if we achieve a good approximation, then our model will also be applicable to the time domain and, in addition, we will have obtained a simple approximation to the Mittag-Leffler function, which is highly demanding from the computational point of view [32,33]. It can help us in computations with fractional-order ZARCs.

4. The compact model. Proposal and results

To obtain a good approximation to the normalized resistance, $\rho_\alpha(w)$, and normalized reactance, $\xi_\alpha(w)$, for the fractional-order ZARC, given in Eqs. (10) and (11), respectively, we had to find parameter values of the multiple-RC network, given in Eqs. (39) and (40), that achieve a match as close as possible between the impedance of the two models in a wide frequency range and for every value of the order exponent α. The procedure that we used is detailed in this section. To do this, some decisions had to be made regarding the range of the normalized angular frequency, w, the range of the order exponent α, the number of RC elements, 2N+1, and the optimization procedure.

Although our model is valid for all frequencies, since we have imposed that it verifies the limits at the extremes of zero and infinity frequencies given in Eqs. (34) and (35), a range of frequencies had to be chosen for the optimization process. For this purpose, we chose a wide range of $w = \omega\tau$, from 10^{-6} to 10^{6}.

The range of the order exponent α is closely related to the number of RC elements, 2N+1, since for α close to 1 a good approximation can be obtained with few RC elements, while much more elements are needed for α values close to zero. Consequently, we had to make a choice about which values of α were used in the optimization procedure, and then we decided on the number of RC elements. Regarding the α

Cuckoo Search via Lévy Flights

Objective function $f(\mathbf{x}), \mathbf{x} = (x_1, ..., x_d)^T$

Generate initial population of n host nests x_i

while (t <MaxGeneration) or (stop criterion)

  Get a cuckoo randomly

  Generate a solution by Lévy flights

  Evaluate its solution quality or objective value f_i

  Choose a nest among n (say, j) randomly

  if ($f_i < f_j$),

    Replace j by the new solution i

  end

  A fraction (p_a) of worse nests are abandoned

  New nests/solutions are built/generated

  Keep best solutions (or nests with quality solutions)

  Rank the solutions and find the current best

  Update $t \leftarrow t + 1$

end while

Postprocess results

Fig. 3. Pseudo code of the Cuckoo search algorithm for a minimization problem [38].

range, our goal was to obtain a model for the ZARC with a fractional-order capacitor, where $0 < \alpha < 1$, with interest in modeling batteries and supercapacitors, where very low values of α, less than 0.3, are unusual. To cite some examples, Farmann et al. [15] optimized the component values of the five RC network in the range 0.45–0.99 of the order exponent, and experimentally measured it in the range 0.35 to 1, approximately. Agudelo et al. [30] provided results in a table in the order range of 0.59 to 0.77, Kim et al. [24] provided results in the order range from 0.7 to 1, and Heil and Jossen [29] provide a result for the 3 RC model valid in the order range of 0.72 to 1. Therefore, we decided to choose the range $0.3 \leq \alpha < 1$ in the optimization procedure. We observed that a model with seven RC elements provided sufficiently accurate results in the range of interest.

And regarding the optimization procedure, due to the high number of adjustment parameters, we opted for a metaheuristic algorithm. In particular, we choose the Cuckoo search algorithm [34,35], as it is simple and performs similar to and even better than other metaheuristic algorithms [36]. This metaheuristic method is nature inspired and is based on the brood parasitism of some cuckoo species. Furthermore, it is enhanced by the Lévy flights rather than by simple isotropic random walks. This algorithm has been used in the context of fractional-order circuits [37], albeit for a different purpose, and we found that it was a suitable option to achieve our target. A pseudo-code of the Cuckoo search algorithm for a minimization problem is shown in Fig. 3 [38].

To apply the optimization procedure, we evenly divided the frequency range in a logarithmic scale and computed the squared difference in the modulus of the impedance measured from the center of the arc in the Nyquist plot (point $(\frac{1}{2}, 0)$) obtained with the two models. The resulting objective function is

$$f_{objective} = \frac{\sqrt{\sum_{j=1} \left(\| Z_{RC}(w_j) - \frac{1}{2} \| - \| Z_\alpha(w_j) - \frac{1}{2} \| \right)^2}}{\xi_{\alpha,max}} \tag{51}$$

Table 1
Parameter expressions as a function of α for the approximation with 5 RC elements.

Parameter	Expression
r_1	$0.186(1-\alpha)^{1.1}$
r_2	$(0.25 + 0.57\alpha^2)(1-\alpha)^{0.72}$
t_1	$\frac{0.045\alpha^{7.32}}{0.04+\alpha^{4.47}}$
t_2	$\frac{0.407\alpha^4}{0.071+\alpha^{2.38}}$

Table 2
Parameter expressions as a function of α for the approximation with 7 RC elements.

Parameter	Expression
r_1	$0.14(1-\alpha)^2$
r_2	$0.22(1-\alpha) - 0.08(1-\alpha)^3$
r_3	$\left(0.12 + 0.057e^{3.4\alpha}\right)(1-\alpha)$
t_1	$1.4 \cdot 10^{-8} e^{19\alpha(1.6-\alpha)}$
t_2	$\frac{0.078\alpha^{5.63}}{0.026+\alpha^{3.67}}$
t_3	$\frac{0.56\alpha^{2.27}}{0.4+\alpha^{1.3}}$

where $\xi_{\alpha,max}$ is given by (12). From now on, we will refer to it as the average relative r.m.s. error.

By applying the Cuckoo search algorithm, initial r_k and t_k values that minimize $f_{objective}$ were found for a set of α values. The optimum parameter values were plotted as a function of α, and then we searched for suitable mathematical expressions to fit this dependence. The result is shown in next subsection.

4.1. The model

The results that we obtained for a network with five RC elements (N=2, four free parameters) are shown in Table 1, and those we obtained for a network with seven RC elements (N=3, six free parameters) are presented in Table 2. In both approximations, the resulting expressions for the resistances are proportional to powers of $1-\alpha$, so that the central RC element, with $r_4 = 1$ and $t = 1$, will be the only element in the limit $\alpha \to 1$.

The average relative r.m.s. error obtained with the equations in Tables 1 and 2 are plotted in Fig. 4. The error is less than 2% for $\alpha > 0.58$ with 5 RC elements, and for $\alpha > 0.48$ with 7 RC elements. It is less than 1% for $\alpha > 0.67$ with the 5RC network and for $\alpha > 0.56$ with the 7RC network. The error is higher with the 5RC network, as expected.

The Nyquist plots for the ZARC and the multiple RC network are shown in Fig. 5 in the cases of 5 RC elements and 7 RC elements, for different α values (0.3, 0.4, 0.5, 0.6, 0.7, 0.8, and 0.9). The real and imaginary parts of the impedance of the ZARC and the multiple RC network with seven RC elements, as a function of the normalized angular frequency, are shown in Fig. 6 for three values of the order exponent α: 0.3, 0.6, and 0.9. From all these results we can conclude that the network with seven RC elements represents a reasonable compromise between accuracy and complexity in the range of interest for fractional-order modeling of batteries and supercapacitors, and for many other applications as well.

A code for the final model, in Octave/Matlab, is provided in Appendix A. Its input is the description of the ZARC by three parameters, α, R, and τ, and gives the values of the seven resistances and the seven capacitances of the 7 RC approximation. If the ZARC is described by the three parameters of Eq. (2), Q is changed by τ by using Eq. (3).

Finally, we can test whether our model, described by the equations given in Tables 1 and 2, can also accurately represent behavior in the time domain. To test the time performance, we have applied a constant current step to the ZARC and to the 5RC and 7RC models described in

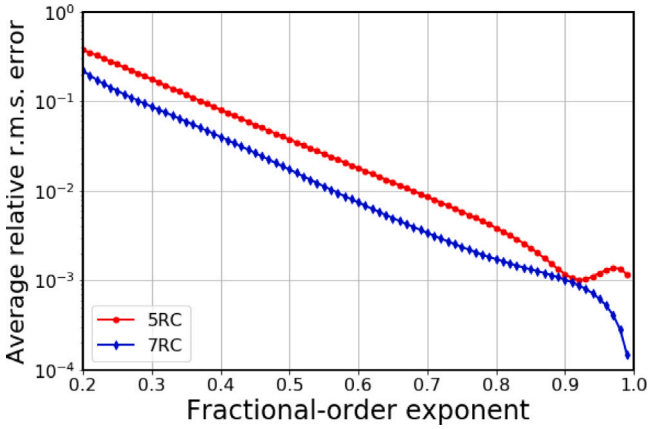

Fig. 4. Average r.m.s. error for the impedance of the multiple RC network with respect to the impedance of the ZARC as a function of the fractional-order exponent for two networks of 5 RC elements and 7 RC elements, respectively.

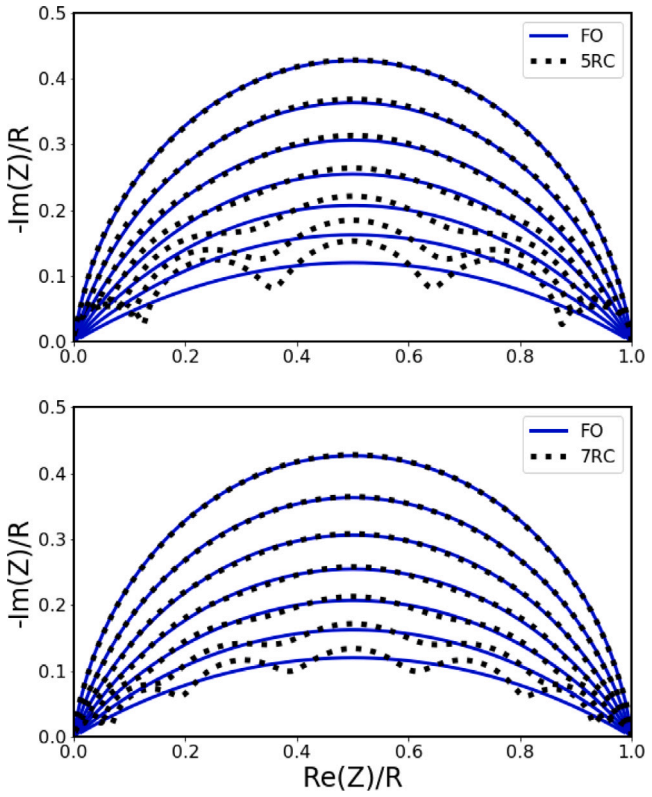

Fig. 5. Nyquist plots for the ZARC and the multiple RC network in two cases, 5RC (top) and 7RC (bottom), for different α values: 0.3, 0.4, 0.5, 0.6, 0.7, 0.8, and 0.9, from down to top. The represented data have been obtained for a normalized angular frequency range from $w = 10^{-6}$ to $w = 10^{6}$.

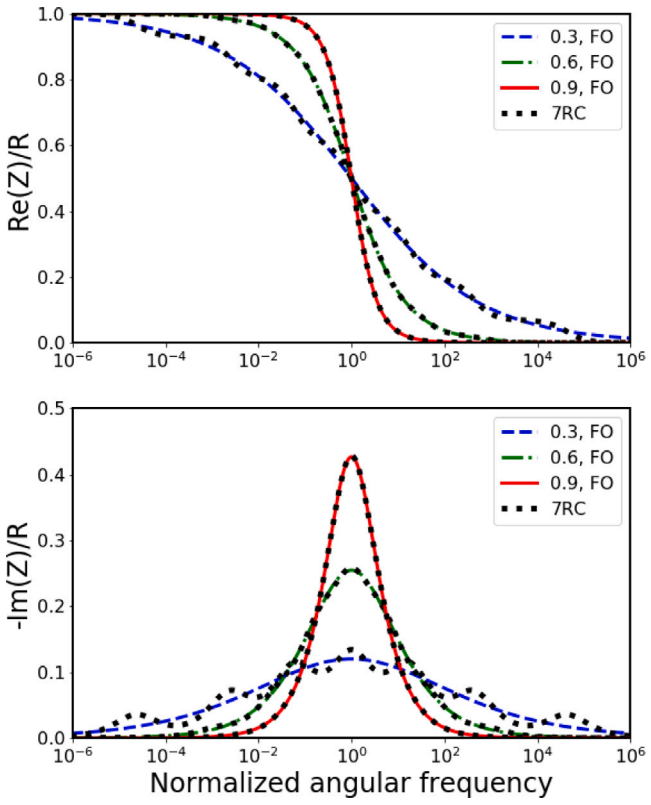

Fig. 6. Real and imaginary parts of the impedance of the ZARC and the multiple RC network with seven RC elements for three α values: 0.3, 0.6, and 0.9.

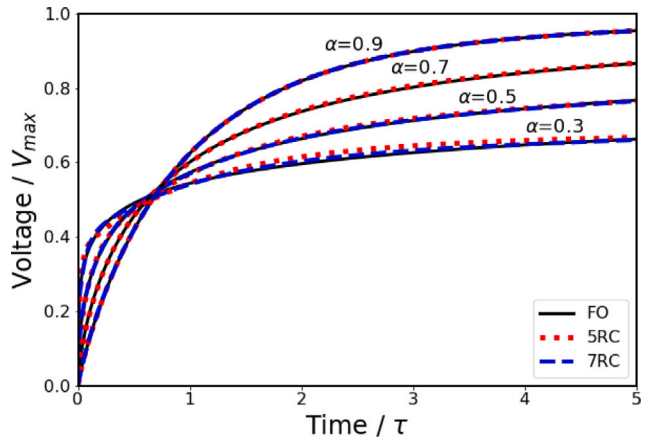

Fig. 7. Response of the ZARC and the 5RC and 7RC models to a step current applied at $t = 0$, up to $t = 5\tau$, for the α values: 0.3, 0.5, 0.7, and 0.9. V_{max} is the maximum voltage that will eventually be reached at $t \to \infty$.

Tables 1 and 2, respectively, and have calculated the voltage response with the three models. The result is shown in Fig. 7. The error is small and will be discussed in next subsection.

A difference with models that do not impose the limits at zero and infinity frequencies would also be noticed in the time domain for very short and long time scales. To verify the performance of our model in these conditions, we applied current pulses of different widths and compared the obtained voltage with that predicted by the fractional-order result given in Eq. (23) in terms of the Mittag-Leffler function. The result is shown in Fig. 8, for $\alpha = 0.5$, and Fig. 9, for $\alpha = 0.7$. Current pulses of widths $t_p = 0.02\tau$, $t_p = 1\tau$, and $t_p = 50\tau$, are applied in the two cases, followed by rest periods of length 0.04τ, 2τ, and 100τ, respectively, with zero current. V_{max} is the maximum voltage that would eventually have been reached at $t \to \infty$ if the current pulse had been maintained. A good agreement can also be observed.

As discussed in Section 3.2, proper behavior is expected in the time domain if the approximation $E_\alpha(-x^\alpha) \approx F_{2N+1}(x)$ in Eq. (49) holds, that is, if the final result of (50) is accurate enough. We have observed that the 7 RC approximation gives us a reasonably good result in a wide range of its argument and a very short computation time. The Mittag-Leffler approximation, evaluated at $-x^\alpha$, can be obtained with the same functions as in Table 2, according to the Octave/Matlab code also provided in Appendix A. The error of this approximation is less

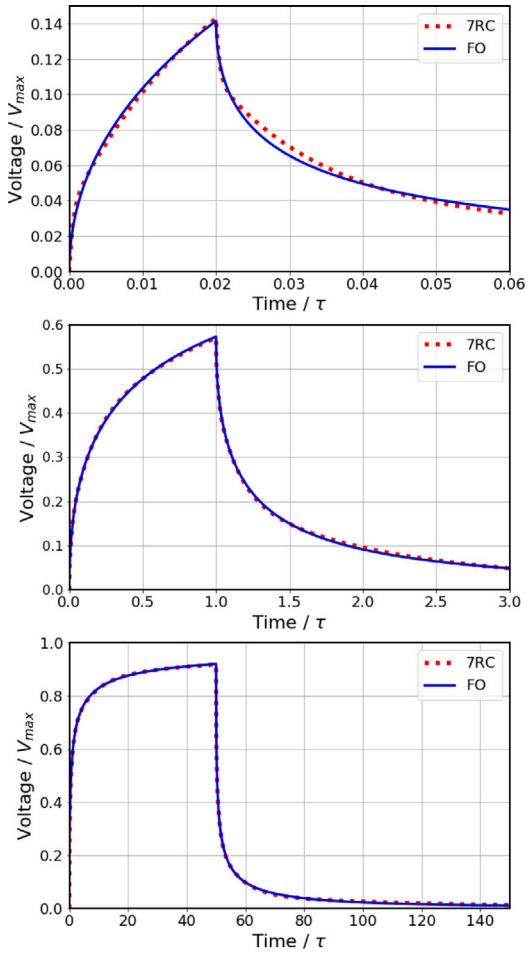

Fig. 8. Response of the ZARC and the 7RC model to a current pulse of width $t_p = 0.02\tau$ (top), $t_p = 1\tau$ (middle), and $t_p = 50\tau$ (bottom), followed by rest periods of duration 0.04τ, 2τ, and 100τ, respectively, with zero current. The order exponent is $\alpha = 0.5$.

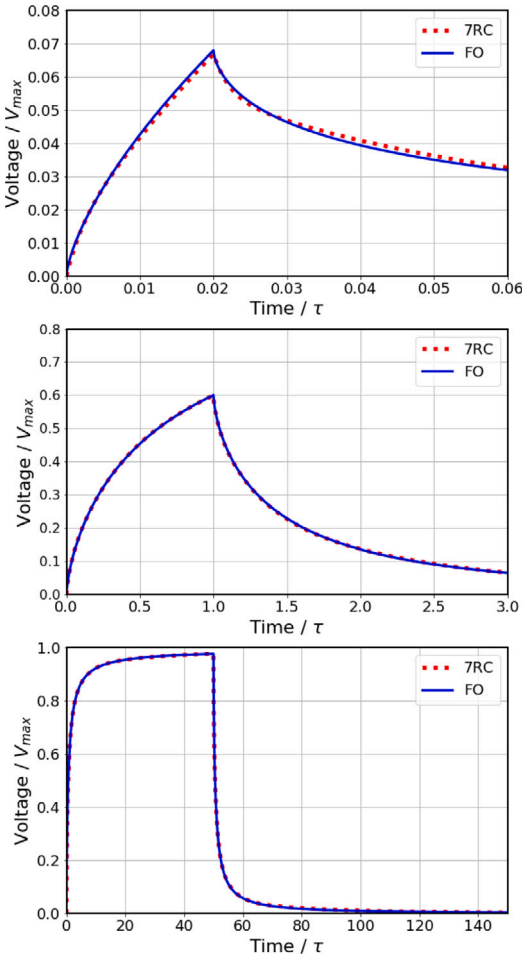

Fig. 9. Response of the ZARC and the 7RC model to a current pulse of width $t_p = 0.02\tau$ (top), $t_p = 1\tau$ (middle), and $t_p = 50\tau$ (bottom), followed by rest periods of duration 0.04τ, 2τ, and 100τ, respectively, with zero current. The order exponent is $\alpha = 0.7$.

than 2% for a wide range of its argument, and less than 1% for a shorter range, depending on the α value. Although this error is higher than that obtained with other excellent procedures that exist in the literature, such as that of Podlubny et al. that we have used for comparison [32], we believe it is accurate enough for many cases where researchers try to adjust experimental results by fractional-order models with comparable accuracy, with the advantage that it requires much less computation time, on the order of 5 times, for $\alpha = 0.9$, to 25 times for $\alpha = 0.3$. This aspect is critical in fractional-order computations where these functions are called repeatedly due to the dependency of the fractional-order models on previous history.

4.2. Comparison with the continuous fraction expansion procedure

As discussed above, there are very useful models that obtain approximations to the ZARC based on passive equivalent circuits, with a continuous dependence on the fractional-order exponent, proposed in the literature [10,25]. In this subsection, we compare our model with five and seven RC elements with a model based on the similar Foster I topology, with five RC elements and a series resistance, and component values obtained with the continuous fraction expansion method [10]. The three equivalent circuit models are shown in Fig. 10.

The normalized component values defined in Eq. (31) are detailed in Table 3 for the three equivalent circuits shown in Fig. 10.

First, the frequency behavior is considered. The Nyquist plot for the two models is shown in Fig. 11(a), with an order value of $\alpha = 0.6$. The

Table 3
Normalized parameter values for the three circuits shown in Fig. 10, for the order-exponent value $\alpha = 0.6$.

Parameter	Foster-I	5 RC	7 RC
r_0	0.0495	–	–
r_1	0.1464	0.0679	0.0224
r_2	0.1951	0.2353	0.0829
r_3	0.2179	0.3936	0.2233
r_4	0.1951	0.2353	0.3427
r_5	0.1464	0.0679	0.2233
r_6	–	–	0.8289
r_7	–	–	0.0224
t_1	0.0816	0.0075	0.0013
t_2	0.3517	0.1435	0.0245
t_3	1.0000	1.0000	0.1920
t_4	2.8432	6.9669	1.0000
t_5	12.260	132.68	5.2085
t_6	–	–	40.806
t_7	–	–	799.68

Foster-I circuit is clearly more accurate in the middle of the curve, but its series resistance makes it less accurate at the extremes, so that it must be used within a frequency band. This band is narrower as the value of exponent α decreases, but a good accuracy is maintained at the center in all cases, while the accuracy of the multiple-RC model decreases with α, but its validity is kept in all the frequency range as seen in Fig. 5.

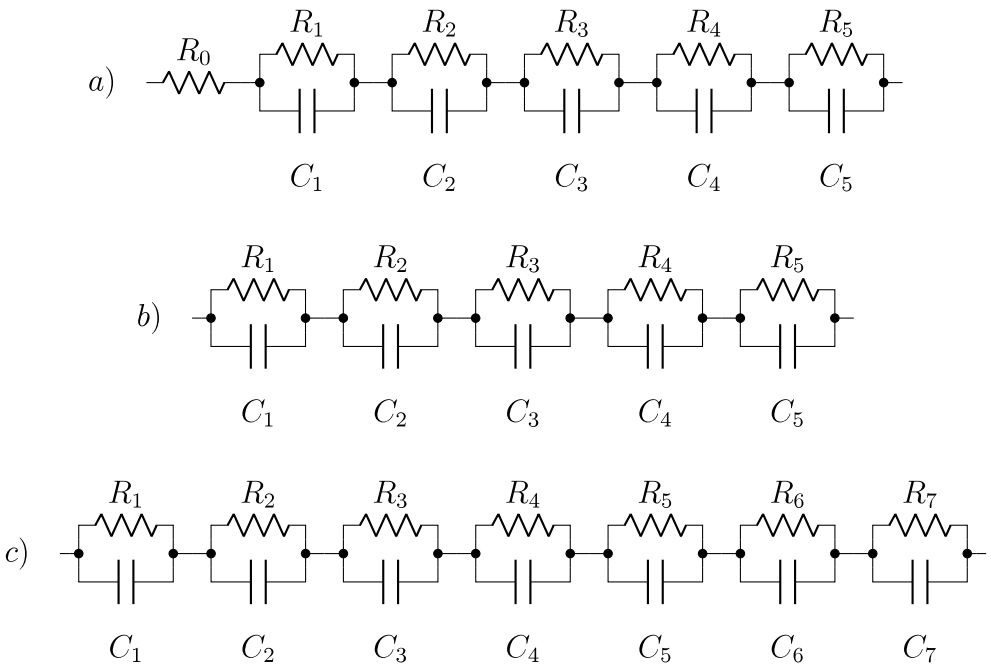

Fig. 10. Equivalent circuit models: (a) Foster-I model with 5 RC elements and continuous-fraction expansion method, (b) multiple-RC model with 5 RC elements, (c) multiple-RC model with 7 RC elements.

These differences in frequency performance are directly translated to the time behavior, as seen in Figs. 11(b) and 11(c), that show the relative error in the voltage calculated after the application of a current step in the time domain, with respect to the fractional-order result based on the Mittag-Leffler function, versus the normalized time ($\frac{t}{\tau}$). The Foster-I circuit is highly accurate in the time range from about 0.15τ to 20τ, approximately, but its error increases outside this range, both at very short and long times. Hence, our 7RC model can be considered as an alternative accurate enough for some applications and has the advantages of its simplicity and its low computational burden. We have tested both models in several applications and have obtained higher computation times with the Foster-I model, ranging from 40% higher to several tens of times longer, depending on the number of times that parameter α is changed and the partial fractional expansion must be performed. Moreover, our model does not need any special function, such as the *residue* function included in Octave/Matlab which may not be available in some circuit simulators to obtain the subcircuit parameters for any value of α. Such subcircuits are demonstrated in the following subsection, in which our model is also compared with Oustaloup's approach, drawing similar conclusions to those obtained in this subsection.

4.3. SPICE model

The equations shown in Table 2 are used in this subsection to build a subcircuit that can be implemented in SPICE (Simulation Program with Integrated Circuits Emphasis). This subcircuit takes the three parameters of the ZARC, namely R, τ, and α as its inputs, and defines the multiple-RN network with seven RC elements. We have named this subcircuit ZARC_UGR, and it is given in Appendix B.

Oustaloup et al. [25] proposed an approach that can also be easily written as a subcircuit. Their model provides the poles and zeros for the approximation to the transfer function of the CPE within a frequency range (ω_b, ω_h) around a central frequency ω_c, and a procedure to easily obtain the component values for the Foster-I topology according to this transfer function. We have also built such a subcircuit, where in addition to the three parameters of the ZARC, a new parameter $B = \omega_h/\omega_c = \omega_c/\omega_b$ has been introduced to define the bandwidth of the approximation, and $\omega_c = 1/\tau$. This subcircuit is composed of a Foster-I

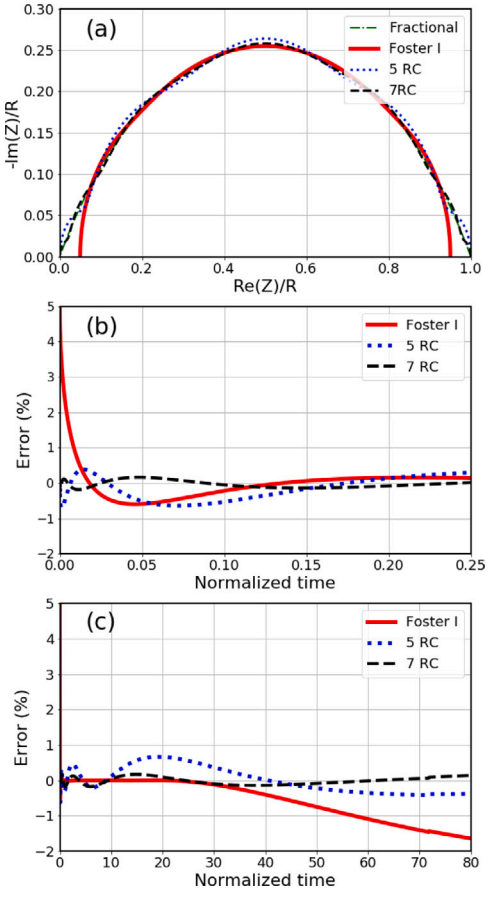

Fig. 11. Comparison of the Foster-I model, obtained with the continuous fraction expansion procedure, in the frequency and time domains for $\alpha = 0.6$. (a) Nyquist plot for a normalized angular frequency range from $w = 10^{-6}$ to $w = 10^{6}$. (b) Step response in the range $(0, 0.25\tau)$. (c) Step response in the range $(0, 80\tau)$.

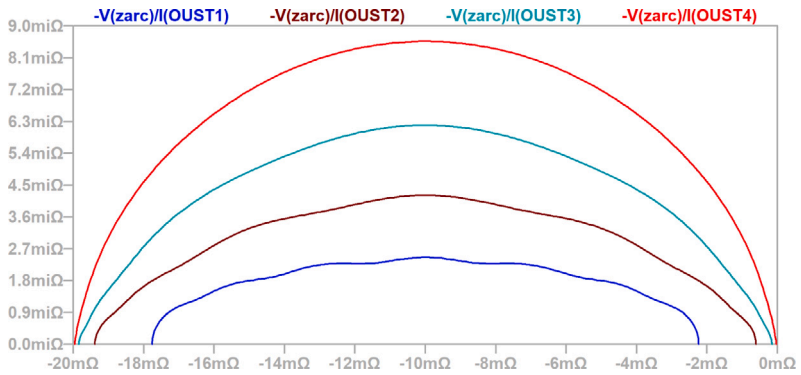

Fig. 12. Nyquist plot for the ZARC_OUST model of the ZARC obtained with LTSPICE for $R = 20$ mΩ, $\tau = 0.1$ s, $B = 1000$, and $\alpha = 0.3, 0.5, 0.7, 0.9$, from bottom to top. A frequency range from 10 μHz to 10 MHz has been chosen in the simulation.

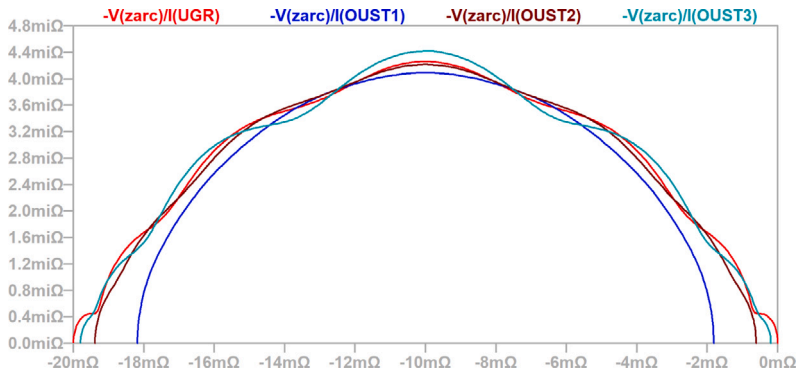

Fig. 13. Nyquist plot for the ZARC_OUST model of the ZARC obtained with LTSPICE for $R = 20$ mΩ, $\tau = 0.1$ s, $\alpha = 0.5$. $B = 100$ for curve OUST1, $B = 1000$ for curve OUST2, and $B = 10000$ for curve OUST3. A frequency range from 10 μHz to 10 MHz has been chosen in the simulation.

circuit with seven RC elements and a series resistance to represent the CPE, and a resistor R in parallel to compose the ZARC. We also provide this subcircuit in Appendix B, with the name ZARC_OUST.

The performance of the two subcircuits has been tested in LTSPICE [39]. The behavior of the ZARC_OUST subcircuit is illustrated in the LTSPICE plot shown in Fig. 12, where the Nyquist plot is represented for $R = 20$ mΩ, $\tau = 0.1$ s, $B = 1000$, and $\alpha = 0.3$, 0.5, 0.7, 0.9, from bottom to top. These values have been chosen since they are within the ranges typically found in battery electric-circuit models, which was the original motivation of our work [8,11], although this choice does not affect our general conclusions.

The curves show less undulations that those provided by our model, but they move away from the limits $(0, 0)$ and $(R, 0)$ as α decreases. This is a consequence of the bandwidth limitation of Oustaloup's approximation, and is less significant as B increases, but then the undulations appear, as shown in Fig. 13, where the Nyquist plots for the ZARC_OUST model with R=20 mΩ, $\tau = 0.1$ s, $\alpha = 0.5$, and $B = 100$, 1000, 10000, are drawn and compared with the result of our model ZARC_UGR. The ripples show up and the extremes approach the limits as B increases, even exceeding those of our model although the limits are not completely reached. The circuit used to obtain these results is shown in Fig. 14.

As we discussed in Section 4.2, the frequency band limits or the series resistance of the Foster-I circuit, have some consequences on the time performance of the Oustaloup model, notably for very short and very long time scales. This is also observed in the LTSPICE simulations. To show this, we have simulated the voltage response of the ZARC to a pulsed current in Fig. 15. Figures (a) and (b) correspond to very short pulses, of width $t_p = 0.02\tau$, and some discontinuities are observed in the pulse edges with the ZARC_OUST model, while the voltage with the ZARC_UGR model is continuous, as the fractional-order voltage is. The voltage step is higher with $\alpha = 0.5$ in figure (a), but it is also observed

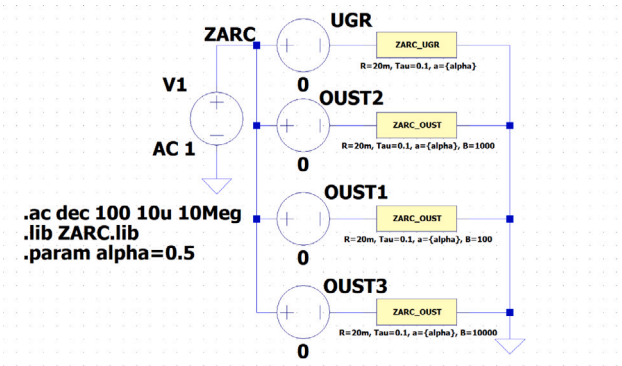

Fig. 14. LTSPICE circuit used to obtain the Nyquist plots for the ZARC_OUST and ZARC_UGR models shown in Fig. 13.

in figure (b) with $\alpha = 0.7$. However, with longer time scales almost no difference is observed with the two models, as shown in figure (c), where the pulse width is $t_p = \tau$.

5. Initialization of ZARC

To obtain the response of the ZARC in time domain in a general situation, the initial condition is a problem. Although the Caputo definition of the fractional derivative has been used very often, since it provides an easy way to deal with the initial voltage, it is not correct as has been demonstrated by several authors [40–42]. In fact, to calculate the voltage from a given time t_0, all the previous history prior to this time must be known since different ways of reaching the initial voltage can produce different subsequent evolution of $v(t)$.

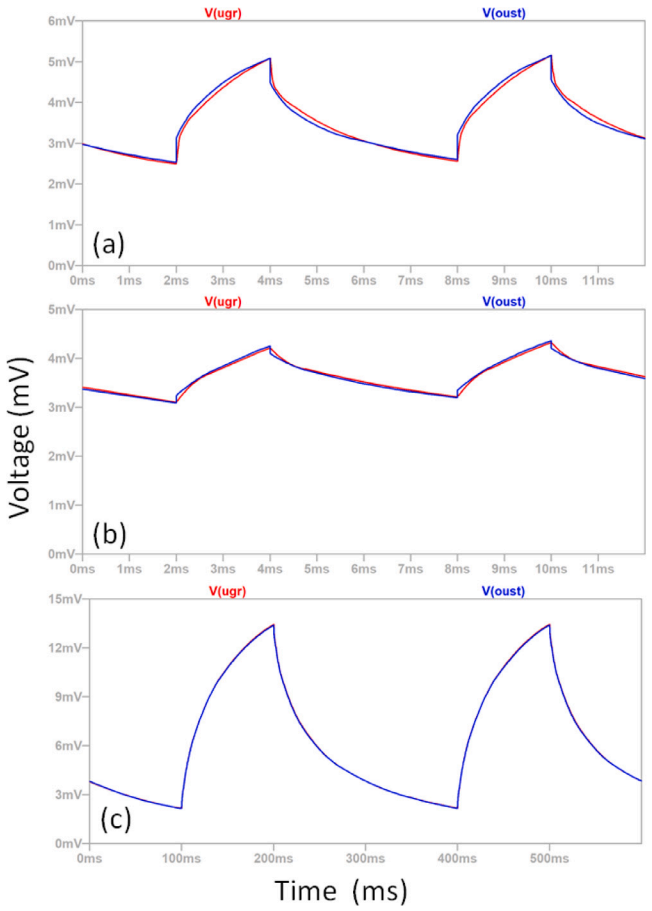

Fig. 15. Voltage response to a pulsed current obtained with LTSPICE for ZARC models with $R = 20$ mΩ and $\tau = 0.1$ s. (a) $\alpha = 0.5$, pulse width $t_p = 0.02\tau$, period 0.06τ; (b) $\alpha = 0.7$, pulse width $t_p = 0.02\tau$, period 0.06τ; (c) $\alpha = 0.7$, pulse width $t_p = \tau$, period 2τ. $B = 1000$ for the ZARC_OUST model.

Since the dependence of previous history is a particular feature of fractional calculus [40,43–46] while the RC element only depends on the initial-voltage value, we could think that the multiple RC approximation solves the initialization problem, but it is only partly solved in fact. The reason of that is that different combinations of the initial voltages of the RC elements that compose the multiple RC model can correspond to the same initial voltage of the whole network, but they lead to different further behavior. This is shown in the following example.

We analyze the case of the decay of the voltage of the ZARC, starting from an initial voltage $v_0 = v(0)$, but considering that this initial voltage has been obtained by different previous histories. We choose $v_0 = 1$ V, but the conclusions will be independent of this choice. Then, we calculate the voltage $v(t)$ for $t \geq 0$, being t the observation time. However, to obtain v_0, we assume that a current I_0 has been applied for a time interval t_0 previous to $t = 0$, starting with a relaxed state with zero initial conditions. Therefore, we define an absolute time, t_a, starting from the relaxed state, so that

$$t_a = t_0 + t \tag{52}$$

For the ZARC model, we apply Eq. (23) in the interval $t_a = 0$ to $t_a = t_0$, which corresponds to $t = 0$.

$$v(t=0) = v(t_a = t_0) = I_0 R \int_0^{t_0} \frac{d}{du} E_\alpha \left[-\left(\frac{t_0 - u}{\tau} \right)^\alpha \right] du, \tag{53}$$

so that

$$v_0 = I_0 R \left\{ 1 - E_\alpha \left[-\left(\frac{t_0}{\tau} \right)^\alpha \right] \right\}. \tag{54}$$

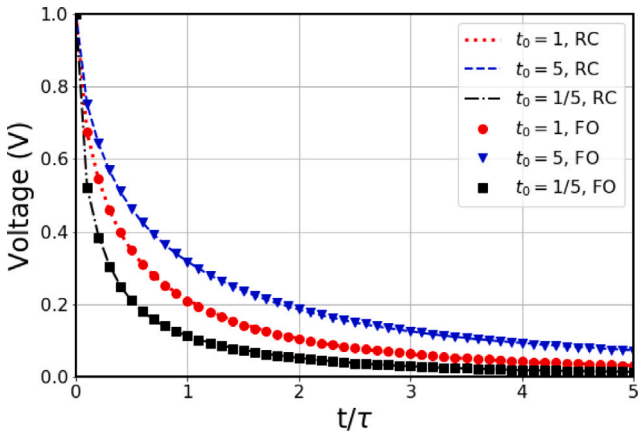

Fig. 16. Different time decays of the voltage of the ZARC models initialized to $v(0) = 1$ V with three different previous currents for three different times: 5τ, τ, and $\frac{\tau}{5}$, respectively. $\alpha = 0.65$.

At $t = 0$ ($t_a = t_0$), the current I_0 is switched off, so that

$$v(t) = v(t_a = t_0 + t) = I_0 R \int_0^{t_0} \frac{d}{du} E_\alpha \left[-\left(\frac{t_0 + t - u}{\tau} \right)^\alpha \right] du, \tag{55}$$

and

$$v(t) = I_0 R \left\{ E_\alpha \left[-\left(\frac{t}{\tau} \right)^\alpha \right] - E_\alpha \left[-\left(\frac{t_0 + t}{\tau} \right)^\alpha \right] \right\}. \tag{56}$$

Combining (54) and (56), we finally obtain

$$v(t) = v_0 \frac{E_\alpha \left[-\left(\frac{t}{\tau} \right)^\alpha \right] - E_\alpha \left[-\left(\frac{t_0 + t}{\tau} \right)^\alpha \right]}{1 - E_\alpha \left[-\left(\frac{t_0}{\tau} \right)^\alpha \right]}, \tag{57}$$

which not only depends on v_0 but also on the time t_0 selected to reach it.

For the multiple RC model, the voltage of each RC element decays exponentially from its initial voltage according to

$$v(t) = \sum_{k=1}^{2N+1} v_k(0) exp\left(-\frac{t}{\tau_k} \right), \tag{58}$$

and the initial voltages are obtained by applying I_0 for t_0. The result is

$$v_k(0) = I_0 R \left[1 - exp\left(-\frac{t_0}{\tau_k} \right) \right], \tag{59}$$

As

$$v_0 = v(t=0) = \sum_{k=1}^{2N+1} v_k(0), \tag{60}$$

we obtain an equation analogous to (57)

$$v(t) = v_0 \frac{\sum_{k=1}^{2N+1} \left[1 - exp\left(-\frac{t_0}{\tau_k} \right) \right] exp\left(-\frac{t}{\tau_k} \right)}{\sum_{k=1}^{2N+1} \left[1 - exp\left(-\frac{t_0}{\tau_k} \right) \right]}, \tag{61}$$

which also depends on t_0.

The results obtained with the two models are shown in Fig. 16 for three initializing times, $t_0 = \tau$, $t_0 = 5\tau$, and $t_0 = \frac{\tau}{5}$. Two facts can be remarked: the dependence of the decay voltage on the previous history, such as expected with fractional-order models as we pointed out in [42], and the very similar results obtained with the two models, which is again a proof of the good behavior of our compact model in the time domain.

Therefore, the multiple RC model does not solve the initialization problem of the ZARC, as expected if we wanted to reproduce its behavior, since although we know the initial voltage, how it is

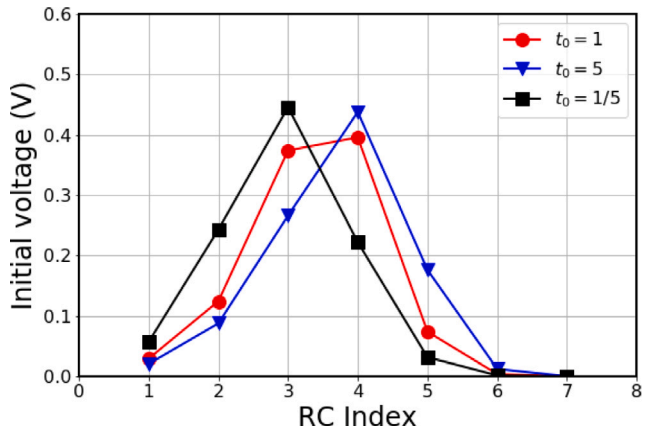

Fig. 17. Different distributions of the initial voltages for the elements of a 7RC network initialized to $v(0) = 1$ V with three different previous currents for three different times: 5τ, τ, and $\frac{\tau}{5}$, and $\alpha = 0.65$.

distributed among the different RC elements actually depends on the previous history. This distribution is shown in Fig. 17 for the three cases represented in Fig. 16. However, we believe the multiple RC model mitigates this problem since only the initial voltages of the seven RC elements are required instead of all the previous history.

6. Conclusions

A compact model for the ZARC has been obtained, based on the multiple-RC approximation. The model starts from a description of the ZARC with three parameters, namely the resistance, the time constant and the order exponent, and provides the values of the resistances and capacitances of an equivalent multiple series RC network. After an optimization process with the Cuckoo search metaheuristic procedure, suitable mathematical functions that provide the values of the circuit parameters for any value of the order exponent α in the range $0 < \alpha < 1$, continuously, have been found. This allows us to use the model in optimization procedures in which the experimental data is fitted by a fractional-order ZARC with a continuous variation of its parameters, and also to implement the model as a subcircuit in circuit simulators.

To obtain the model, we have analyzed the ZARC and multiple RC models with similar procedures and definitions, both in the frequency domain and in the time domain, in a normalized way, so that the two models are compared regardless of the particular values of the resistance and the time constant, and useful equations are obtained, in particular an approximation of the Mittag-Leffler function which is obtained as a solution of the differential equation for the ZARC.

The validity of the model has been verified by calculations in the frequency and time domains. It has also been compared with the results of models based on a transfer-function approximation that led to a Foster-I circuit by a continuous fraction expansion procedure. The models have been compared by using Octave calculations and SPICE simulations. The Octave/Matlab functions developed for our model and the subcircuits we have defined for both our model and Oustaloup's approach are provided.

As a final application of our model, it has been compared with the fractional-order model in relation to the ZARC initialization problem, and we have shown that both produce similar results, but the multiple RC model with seven RC elements only needs seven parameters for its initialization instead of the whole previous history that the fractional-order model requires.

The model can be useful for calculations and simulations of fractional-order elements in the battery and supercapacitor field, but also in various other applications where fractional calculus is used.

Declaration of competing interest

The authors declare that they have no known competing financial interests or personal relationships that could have appeared to influence the work reported in this paper.

Acknowledgements

Funding for open access charge: Universidad de Granada / CBUA.

Appendix A

Function codes in Octave/Matlab:

```
function P = Zarc_7RC(alpha, R, tau)
% Function to obtain the resistance and capacitance values of
% the 7RC model of the ZARC, defined by three parameters
% P(:,1) contains R1 to R7
% P(:,2) contains C1 to C7
r(1)=0.14*(1-alpha)^2;
r(2)=0.22*(1-alpha)-0.08*(1-alpha)^3;
r(3)=(0.12+0.057*exp(3.4*alpha))*(1-alpha);
t(1)=1.4e-8*exp(19*alpha*(1.6-alpha));
t(2)=(0.078*alpha^5.63)/(0.026+alpha^3.67);
t(3)=0.56*alpha^2.27/(0.4+alpha^1.3);
r(7)=r(1);
r(6)=r(2);
r(5)=r(3);
r(4)=1-2*(r(1)+r(2)+r(3));
t(7)=1/t(1);
t(6)=1/t(2);
t(5)=1/t(3);
t(4)=1;
P(:,1)=r*R;
P(:,2)=(t./r)*(tau/R);
endfunction
function E = ML7RC(a, x)
% Approximation to the Mittag-Leffler function evaluated at -x^a
% Warning!! It does not provide ML_a(x) but ML_a(-x^a)!!!
A1=0.14*(1-a)^2;
A2=0.22*(1-a)-0.08*(1-a)^3;
A3=(0.12+0.057*exp(3.4*a))*(1-a);
A4=1.4e-8*exp(19*a*(1.6-a));
A5=(0.078*a^5.63)/(0.026+a^3.67);
A6=0.56*a^2.27/(0.4+a^1.3);
E=exp(-x)-A1*(2*exp(-x)-exp(-x/A4)-exp(-x*A4));
E=E-A2*(2*exp(-x)-exp(-x/A5)-exp(-x*A5))-A3*(2*exp(-x)
-exp(-x/A6)-exp(-x*A6));
endfunction
```

Appendix B

```
SPICE subcircuits for the ZARC:
.subckt ZARC_UGR n1 n2
**********************************
*** Input parameters ***
.param R=1
.param Tau=1
.param a=0.5
*** Model components ****
.param r11=0.14*(1-a)**2
.param r22=0.22*(1-a)-0.08*(1-a)**3
.param r33=(0.12+0.057*exp(3.4*a))*(1-a)
.param t11=1.4e-8*exp(19*a*(1.6-a))
.param t22=(0.078*a**5.63)/(0.026+a**3.67)
.param t33=0.56*a**2.27/(0.4+a**1.3)
.param r77=r11
```

```
.param r66=r22
.param r55=r33
.param r44=1-2*(r11+r22+r33)
.param t77=1/t11;
.param t66=1/t22;
.param t55=1/t33;
.param t44=1;
*** Circuit ***
R1 n1 n3 {r11*R}
R2 n3 n4 {r22*R}
R3 n4 n5 {r33*R}
R4 n5 n6 {r44*R}
R5 n6 n7 {r55*R}
R6 n7 n8 {r66*R}
R7 n8 n2 {r77*R}
C1 n1 n3 {t11/r11*Tau/R}
C2 n3 n4 {t22/r22*Tau/R}
C3 n4 n5 {t33/r33*Tau/R}
C4 n5 n6 {t44/r44*Tau/R}
C5 n6 n7 {t55/r55*Tau/R}
C6 n7 n8 {t66/r66*Tau/R}
C7 n8 n2 {t77/r77*Tau/R}
.ends ZARC_UGR
***************************************
***************************************
.subckt ZARC_OUST n1 n2
*** Input parameters ***
.param R=1
.param Tau=1
.param a=0.5
.param B=1e3;
*** Model components ****
.param rn0=B**(-a)
.param g=B**(-2/7)
.param K=B**a*(1-g**a)
.param tn4=B**(a/7)
.param tn1=tn4/g**3
.param tn2=tn4/g**2
.param tn3=tn4/g
.param tn5=tn4*g
.param tn6=tn4*g**2
.param tn7=tn4*g**3
.param rn1=K*(1-g**(a+1))/(1-g)*(1-g**(a+2))/(1-g**2)*
+   (1-g**(a+3))/(1-g**3)*(1-g**(a+4))/(1-g**4)*
+   (1-g**(a+5))/(1-g**5)*(1-g**(a+6))/(1-g**6)
.param rn2=K*(g**a-g)/(1-g)*(1-g**(a+1))/(1-g)*
+   (1-g**(a+2))/(1-g**2)*(1-g**(a+3))/(1-g**3)*
+   (1-g**(a+4))/(1-g**4)*(1-g**(a+5))/(1-g**5)
.param rn3=K*(g**a-g**2)/(1-g**2)*(g**a-g)/(1-g)*
+   (1-g**(a+1))/(1-g)*(1-g**(a+2))/(1-g**2)*
+   (1-g**(a+3))/(1-g**3)*(1-g**(a+4))/(1-g**4)
.param rn4=K*(g**a-g**3)/(1-g**3)*(g**a-g**2)/
+   (1-g**2)*(g**a-g)/(1-g)*(1-g**(a+1))/(1-g)*
+   (1-g**(a+2))/(1-g**2)*(1-g**(a+3))/(1-g**3)
.param rn5=K*(g**a-g**4)/(1-g**4)*(g**a-g**3)/(1-g**3)*
+   (g**a-g**2)/(1-g**2)*(g**a-g)/(1-g)*(1-g**(a+1))
+   /(1-g)*(1-g**(a+2))/(1-g**2)
.param rn6=K*(g**a-g**5)/(1-g**5)*(g**a-g**4)/(1-g**4)*
+   (g**a-g**3)/(1-g**3)*(g**a-g**2)/(1-g**2)*
+   (g**a-g)/(1-g)*(1-g**(a+1))/(1-g)
.param rn7=K*(g**a-g**6)/(1-g**6)*(g**a-g**5)/(1-g**5)*
+   (g**a-g**4)/(1-g**4)*(g**a-g**3)/(1-g**3)*
+   (g**a-g**2)/(1-g**2)*(g**a-g)/(1-g)
*** Circuit ***
Rpar n1 n2 {R}
R0 n1 n0 {rn0*R}
R1 n0 n3 {rn1*R}
R2 n3 n4 {rn2*R}
R3 n4 n5 {rn3*R}
R4 n5 n6 {rn4*R}
R5 n6 n7 {rn5*R}
R6 n7 n8 {rn6*R}
R7 n8 n2 {rn7*R}
C1 n0 n3 {tn1/rn1*Tau/R}
C2 n3 n4 {tn2/rn2*Tau/R}
C3 n4 n5 {tn3/rn3*Tau/R}
C4 n5 n6 {tn4/rn4*Tau/R}
C5 n6 n7 {tn5/rn5*Tau/R}
C6 n7 n8 {tn6/rn6*Tau/R}
C7 n8 n2 {tn7/rn7*Tau/R}
.ends ZARC_OUST
***************************************
```

References

[1] Podlubny I. Fractional differential equations: An Introduction to fraction derivatives, fractional differential equations, to methods of their solution and some of their applications. San Diego: Academic Press; 1999, p. 1–316.

[2] Elwakil AS. Fractional-order circuits and systems: An emerging interdisciplinary research area. IEEE Circuits Syst Mag 2010;10(4):40–50. http://dx.doi.org/10.1109/MCAS.2010.938637.

[3] Ionescu C, Lopes A, Copot D, Machado J, Bates J. The role of fractional calculus in modeling biological phenomena: A review. Commun Nonlinear Sci Numer Simul 2017;51:141–59. http://dx.doi.org/10.1016/j.cnsns.2017.04.001, URL https://www.sciencedirect.com/science/article/pii/S1007570417301119.

[4] Kapoulea S, Psychalinos C, Elwakil AS. Simple implementations of fractional-order driving-point impedances: Application to biological tissue models. AEU - Int J Electron Commun 2021;137:153784. http://dx.doi.org/10.1016/j.aeue.2021.153784, URL https://www.sciencedirect.com/science/article/pii/S1434841121001813.

[5] Bertsias P, Kapoulea S, Psychalinos C, Elwakil AS. Chapter two - A collection of interdisciplinary applications of fractional-order circuits. In: Radwan AG, Khanday FA, Said LA, editors. Fractional order systems. Emerging methodologies and applications in modelling, vol. 1, Academic Press; 2022, p. 35–69. http://dx.doi.org/10.1016/B978-0-12-824293-3.00007-7, URL https://www.sciencedirect.com/science/article/pii/B9780128242933000077.

[6] Mijat N, Jurisic D, Moschytz GS. Analog modeling of fractional-order elements: A classical circuit theory approach. IEEE Access 2021;9:110309–31. http://dx.doi.org/10.1109/ACCESS.2021.3101160.

[7] Fricke H. XXXIII. The theory of electrolytic polarization. Lond, Edinb Dublin Philos Mag J Sci 1932;14(90):310–8. http://dx.doi.org/10.1080/14786443209462064.

[8] Andre D, Meiler M, Steiner K, Walz H, Soczka-Guth T, Sauer DU. Characterization of high-power lithium-ion batteries by electrochemical impedance spectroscopy. II: Modelling. J Power Sources 2011;196(12):5349–56. http://dx.doi.org/10.1016/j.jpowsour.2010.07.071.

[9] Fouda ME, Allagui A, Elwakil AS, Das S, Psychalinos C, Radwan AG. Nonlinear charge-voltage relationship in constant phase element. AEU-Int J Electron Commun 2020;117:153104. http://dx.doi.org/10.1016/j.aeue.2020.153104.

[10] Tsirimokou G. A systematic procedure for deriving RC networks of fractional-order elements emulators using MATLAB. AEU - Int J Electron Commun 2017;78:7–14. http://dx.doi.org/10.1016/j.aeue.2017.05.003, URL https://www.sciencedirect.com/science/article/pii/S1434841117305800.

[11] Gagneur L, Driemeyer-Franco A, Forgez C, Friedrich G. Modeling of the diffusion phenomenon in a lithium-ion cell using frequency or time domain identification. Microelectron Reliab 2013;53:784–96. http://dx.doi.org/10.1016/j.microrel.2013.03.009.

[12] Plett GL. Battery management systems, Vol I: Battery modeling. Artech House Power Engineering Series; 2015, p. 1–327.

[13] Macdonald JR. New aspects of some small-signal ac frequency response functions. Solid-State Ionics 1985;15(2):159–61. http://dx.doi.org/10.1016/0167-2738(85)90095-5.

[14] Wang B, Li SE, Peng H, Liu Z. Fractional-order modeling and parameter identification for lithium-ion batteries. J Power Sources 2015;293:151–61. http://dx.doi.org/10.1016/j.jpowsour.2015.05.059.

[15] Farmann A, Waag W, Sauer DU. Adaptive approach for on-board impedance parameters and voltage estimation of lithium-ion batteries in electric vehicles. J Power Sources 2015;299:176–88. http://dx.doi.org/10.1016/j.jpowsour.2015.08.087, URL https://www.sciencedirect.com/science/article/pii/S037877531530241X.

[16] Krewer U, Röder F, Harinath E, Braatz RD, Bedürftig B, Findeisen R. Review—dynamic models of li-ion batteries for diagnosis and operation: A review and perspective. J Electrochem Soc 2018;165(16):A3656–73. http://dx.doi.org/10.1149/2.1061814jes.

[17] Nasser-Eddine A, Huard B, Gabano J-D, Poinot T, Martemianov S, Thomas A. Fast time domain identification of electrochemical systems at low frequencies using fractional modeling. J Electroanal Soc 2020;862:113957. http://dx.doi.org/10.1016/j.jelechem.2020.113957.

[18] Hernández-Balaguera E. Numerical approximations on the transient analysis of bioelectric phenomena at long time scales via the Mittag-Leffler function. Chaos Solitons Fractals 2021;145:110768. http://dx.doi.org/10.1016/j.chaos.2021.110768, URL https://www.sciencedirect.com/science/article/pii/S096007792100120X.

[19] Petras I. Fractional-order nonlinear systems. Modeling, analysis and simulation. Berlin Heidelberg: Springer-Verlag; 2011.

[20] Domansky O, Sotner R, Langhammer L, Jerabek J, Psychalinos C, Tsirimokou G. Practical design of RC approximants of constant phase elements and Their Implementation in fractional-order PID regulators using CMOS voltage differencing current conveyors. Circuits Systems Signal Process 2019;38(4):1520–46. http://dx.doi.org/10.1007/s00034-018-0944-z.

[21] Bertrand N, Sabatier J, Briat O, Vinassa J-M. Embedded fractional nonlinear supercapacitor model and its parametric estimation method. IEEE Trans Ind Electron 2010;57:3991–4000. http://dx.doi.org/10.1109/TIE.2010.2076307.

[22] Alavi SMM, Birkl CR, Howey DA. Time-domain fitting of battery electrochemical impedance models. J Power Sources 2015;288:345–52. http://dx.doi.org/10.1016/j.jpowsour.2015.04.099.

[23] Nasser-Eddine A, Huard B, Gabano J-D, Poinot T. A two steps method for electrochemical impedance modeling using fractional order system in time and frequency domains. Control Eng Pract 2019;86:96–104. http://dx.doi.org/10.1016/j.conengprac.2019.03.001.

[24] Kim S-H, Choi W, Lee K-B, Choi S. Advanced dynamic simulation of supercapacitors considering parameter variation and self-discharge. IEEE Trans Power Electron 2011;26(11):3377–85. http://dx.doi.org/10.1109/TPEL.2011.2136388.

[25] Oustaloup A, Levron F, Mathieu B, Nanot F. Frequency-band complex noninteger differentiator: Characterization and synthesis. IEEE Trans Circuits Syst I 2000;47:25–30. http://dx.doi.org/10.1109/81.817385.

[26] Nasser Eddine A, Huard B, Gabano J-D, Poinot T. Initialization of a fractional order identification algorithm applied for lithium-ion battery modeling in time domain. Commun Nonlinear Sci Numer Simul 2018;59:375–86. http://dx.doi.org/10.1016/j.cnsns.2017.11.034, URL https://www.sciencedirect.com/science/article/pii/S1007570417304227.

[27] Walia MS, Garg R, Goyal P. Electronic and material realizations of fractional-order elements. Mater Today: Proc 2021;45:5342–6. http://dx.doi.org/10.1016/j.matpr.2021.01.924, Second International Conference on Aspects of Materials Science and Engineering (ICAMSE 2021), URL https://www.sciencedirect.com/science/article/pii/S221478532101021X.

[28] Ren H, Zhao Y, Chen S, Yang LA. A comparative study of lumped equivalent circuit models of a lithium battery for state of charge prediction. Int J Energy Res 2019;43:7306–15. http://dx.doi.org/10.1002/er.4759.

[29] Heil T, Jossen A. Continuous approximation of the ZARC element with passive components. Meas Sci Technol 2021;32(10):104011. http://dx.doi.org/10.1088/1361-6501/ac0466.

[30] Agudelo BO, Zamboni W, Monmasson E. A comparison of time-domain implementation methods for fractional-order battery impedance models. Energies 2021;14:4415. http://dx.doi.org/10.3390/en14154415.

[31] Dyke PPG. An introduction to laplace transforms and fourier series. London, Berlin, Heidelberg: Springer-Verlag; 2001, p. 37–75.

[32] Podlubny I, Petráš I, Skovranek T, Terpák J. Toolboxes and programs for fractional-order system identification, modeling, simulation, and control. In: 2016 17th International Carpathian control conference. 2016, p. 608–12. http://dx.doi.org/10.1109/CarpathianCC.2016.7501168.

[33] Sarumi IO, Furati KM, Khaliq AQM. Highly accurate global padé approximations of generalized Mittag–Leffler function and its inverse. J Sci Comput 2020;82(2):46. http://dx.doi.org/10.1007/s10915-020-01150-y.

[34] Yang X-S, Deb S. Cuckoo search via Lévy flights. In: 2009 World congress on nature biologically inspired computing. 2009, p. 210–4. http://dx.doi.org/10.1109/NABIC.2009.5393690.

[35] Yang X-S, Deb S. Engineering optimization by cuckoo search. Int J Math Model Numer Optim 2010;1(4):330–43, URL http://arxiv.org/PS_cache/arxiv/pdf/1005/1005.2908v2.pdf.

[36] Civicioglu P, Besdok E. A conceptual comparison of the cuckoo-search, particle swarm optimization, differential evolution and artificial bee colony algorithms. Artif Intell Rev 2013;39(4):315–46. http://dx.doi.org/10.1007/s10462-011-9276-0.

[37] AbdelAty A, Fouda ME, Elbarawy MT, Radwan A. Optimal charging of fractional-order circuits with cuckoo search. J Adv Res 2021;32:119–31. http://dx.doi.org/10.1016/j.jare.2020.11.014, Fractional Calculus Models for the Dynamics of Complex System, URL https://www.sciencedirect.com/science/article/pii/S2090123220302484.

[38] Yang X-S. Chapter 9 - cuckoo search. In: Yang X-S, editor. Nature-inspired optimization algorithms. Oxford: Elsevier; 2014, p. 129–39. http://dx.doi.org/10.1016/B978-0-12-416743-8.00009-9, URL https://www.sciencedirect.com/science/article/pii/B9780124167438000099.

[39] LTSpice. 2022, https://www.analog.com/en/design-center/design-tools-and-calculators/ltspice-simulator.html. [Accessed 28 March 2022].

[40] Hartley T, Lorenzo C. Dynamics and control of initialized fractional-order systems. Nonlinear Dynam 2002;29(1–4):201–33. http://dx.doi.org/10.1023/A:1016534921583.

[41] Sabatier J, Farges C. Initial value problems should not be associated to fractional model descriptions whatever the derivative definition used. AIMS Math 2021;6:11318. http://dx.doi.org/10.3934/math.2021657, URL: https://www.aimspress.com/article/doi/10.3934/math.2021657.

[42] López-Villanueva JA, Rodríguez Bolívar S. Constant phase element in the time domain: The problem of initialization. Energies 2022;15(3):792. http://dx.doi.org/10.3390/en15030792.

[43] Fukunaga M, Shimizu N. Role of prehistories in the initial value problems of fractional viscoelastic equations. Nonlinear Dynam 2004;38:207–20. http://dx.doi.org/10.1007/s11071-004-3756-6.

[44] Du ML, Wang ZH. Initialized fractional differential equations with Riemann-Liouville fractional-order derivative. Eur Phys J Spec Top 2011;193:49–60. http://dx.doi.org/10.1140/epjst/e2011-01380-8.

[45] Du B, Wei Y, Liang S, Wang Y. Estimation of exact initial states of fractional order systems. Nonlinear Dynam 2016;86:2061–170. http://dx.doi.org/10.1007/s11071-016-3015-7.

[46] Trigeassou J, Maamri N. Initial conditions and initialization of linear fractional differential equations. Signal Process 2011;91(3):427–36. http://dx.doi.org/10.1016/j.sigpro.2010.03.010.